Chapter 8
Graphene for Biomedical Applications

Yufei Ma, Jie Huang, He Shen, Mengxin Zhang, Saijie Song and Zhijun Zhang

Graphene is a one-atom-thick sheet of sp^2 carbon atoms with hexagonal lattice. The unique two-dimensional (2D) structure of graphene and its distinctive electrical features owing to numerous free electrons have been attracting increasing interests in the field of electronics [1], sensors [2], energy [3], etc., since its discovery in 2004 [4]. In addition, due to its ultralarge surface area and unique optical properties, graphene and its derivatives triggered massive explorations in environmental [5] and biomedical applications [6, 7]. In this chapter, we survey the emerging applications of graphene and its related derivatives in the field of biology and medicine, including drug delivery, therapeutics, imaging and sensing, as well as cell culture substrates and antibacterial performance.

8.1 Preparation and Modification

Most of the biological incidents occur in physiological conditions which normally require good aqueous stability in terms of graphene's biomedical applications. In order to obtain excellent physiological stability, graphene oxide (GO), a very important derivative of graphene, is usually used. To date, various oxidative protocols for gram-scaled GO preparation from graphite have been developed [8], including Brodie's method (formic HNO_3 and $KClO_3$), Hummer's method ($KMnO_4$ and H_2SO_4), and Marcano's method (H_2SO_4 and H_3PO_4). Although nice control over the quality and reproducibility has always been a challenge, GO samples with various lateral size, oxygen content, functional groups, and thus biocompatibility can be synthesized by tuning the synthetic routes. Among them, a modified Hummer's method is widely used for further biomedical applications of GO, due to its mild reaction condition and relatively facile preparation. A typical synthetic procedure consists of pre-oxidation of graphite with concentrated H_2SO_4, $K_2S_2O_8$, and P_2O_5, subsequent oxidation with H_2SO_4 and $KMnO_4$, followed by mediation with H_2O_2

Z. Zhang (✉) · Y. Ma · J. Huang · H. Shen · M. Zhang · S. Song
CAS Key Laboratory of Nano-Bio Interface, Suzhou Key Laboratory for Nanotheranostics, Division of Nanobiomedicine, Suzhou Institute of Nano-Tech and Nano-Bionics, Chinese Academy of Sciences, Suzhou 215123, China
e-mail: zjzhang2007@sinano.ac.cn

M. Zhang et al. (eds.), *Carbon Nanomaterials for Biomedical Applications,*
Springer Series in Biomaterials Science and Engineering 5,
DOI 10.1007/978-3-319-22861-7_8

and elimination of metal ions with dilute HCl, ultrasonic exfoliation, and final purification through dialysis [9].

The physiological stability of bare GO rarely meets the needs of biomedical study, since it still possesses a large surface area and a strong π–π interaction for self-aggregation. Therefore, GO preparations for biological studies involve further steps, such as surface passivation (such as polymer modification and phospholipids coating) and size reduction (resulting deficient attraction against Brownian motion). For example, functionalization of GO by polyethylene glycol (PEG), polyethylenimine (PEI), dextran, and hyaluronic acid (HA) can significantly improve the biocompatibility of GO; ultrasmall GO (usGO < 10 nm), also named with graphene quantum dots (GQD) due to its inherent fluorescence, displays no obvious in vitro and in vivo toxicity [10]; moreover, a branched polymer (six-armed PEG) coating facilitates the size reduction of GO under ultrasonic condition, resulting in a GO with small size (10–30 nm) [11].

In some cases, GO can be reduced using $NaBH_4$, N_2H_4, or $NH_3 \cdot H_2O$, generating reduced GO (rGO). The reduction greatly decreases oxygen-containing functional groups on GO surface, enabling rGO with enhanced adsorbing ability, increased near-infrared (NIR) absorbance, and improved charge mobility. With no doubt, rGO needs further modification with hydrophilic polymers to be used in biomedical fields, such as drug delivery and photothermal or photodynamic therapies.

8.2 Graphene-based Therapeutics

As unique two-dimensional (2D) nanomaterials, graphene and its derivatives (especially GO) benefit from their large surface area, and thus have been extensively explored as a versatile platform for the deliberate delivery of drugs, proteins, and genes. Moreover, GO displays strong absorption in the NIR region, attracting much attention for its potentials in photothermal and photodynamic therapies, as well as photoacoustic imaging.

8.2.1 GO for Drug Delivery

GO, as a representative member among the family of graphene-based nanomaterials, has abundant functional groups (such as hydroxyl, carboxyl, carbonyl, and epoxy groups) for flexible modification, as well as high specific surface area for excellent loading capacity. Therefore, GO and rGO show potential application in drug delivery as long as their physiological stability is improved through conjugation with hydrophilic molecules.

Dai et al. first reported the use of GO as a drug delivery system in 2008, opening up the application of GO in biomedical field. Their pioneering study demonstrated the feasibility of nanoscale GO (NGO) as a novel nanocarrier for efficient loading and delivery of hydrophobic aromatic anticancer drugs into cells. NGO was first

modified with an amine-terminated six-armed PEG molecule, and then loaded with SN38, a hydrophobic camptothecin (CPT) analogue, via non-covalent π–π stacking interaction. The NGO/SN38 complex showed excellent aqueous solubility and high cytotoxicity for HCT-116 cells. Moreover, the same group anchored rituxan (CD 20^+ antibody) for targeted delivery of doxorubicin (DOX) into cells, and showed a pH-dependent drug release due to π–π stacking interaction between DOX and NGO [11]. Similarly, Zhang group also demonstrated that the release of DOX from GO surface was pH-responded, through tracking the surface-enhanced Raman spectroscopy (SERS) signal of DOX loaded on Ag–GO. As the results suggested, Ag–GO/DOX was taken up by cells through endocytosis and then captured into the lysosomes, followed by DOX detaching from GO and escaping from the lysosomes into the cytoplasm in an acidic environment [12].

To efficiently deliver drug molecules to a specific tumor site and reduce the toxicity to normal cells, Yang et al. grafted adamantane-modified porphyrin on GO via π–π stacking between porphyrin and GO, and then folic acid (FA)-modified β-cyclodextrin (β-CD) through the hydrophobic interaction between CD cavity and adamantane. DOX was loaded on the composites, which could specifically target to the tumor cells and exhibited significant antitumor effect to HeLa cells. Meanwhile, DOX loaded on this nanocarrier showed much lower toxicity to normal cells (cell viability 97%, 24 h) than that of free DOX (cell viability 57%, 24 h), indicating this GO nanocomposites to be promising in the clinical cancer therapy with fine biosafety [13].

Controlled loading and targeted delivery of multiple drugs is widely accepted by clinical practice in cancer therapy, in order to weaken the drug resistance of cancer cells and finally enhance the antitumor effect [14]. In order to achieve an enhanced efficacy, Zhang et al. explored the feasibility of GO as a nanocarrier for delivery of multiple anticancer drugs (Fig. 8.1) [9, 15]. In their study, NGO was functionalized with sulfonic acid groups to improve the physiological stability and with FA molecule to allow targeted delivery of anticancer drugs into human breast cancer cells (MCF-7 cells, with FA receptors). Then two common anticancer drugs, DOX and CPT, were loaded onto this FA-conjugated NGO via π–π interaction. NGO could load DOX as much as fourfold of its own weight, while the loading payload of CPT was only 4.5%. Different loading ability of GO for these two drugs was ascribed to the difference in chemical structures of the two drugs and thus in the interactions between GO and drug molecules. In addition, the loading ratio of GO was linearly correlated to the concentration of DOX, indicating possibility of controlled loading and targeted delivery simultaneously. Compared with single drug loaded onto NGO, co-delivery of DOX and CPT with NGO induced much higher cytotoxicity to cancer cells [9].

8.2.2 GO for Gene Delivery

Gene therapy is a promising approach to treat multifarious diseases caused by gene damage, for example, cancer. Compared to current antitumor therapies, gene ther-

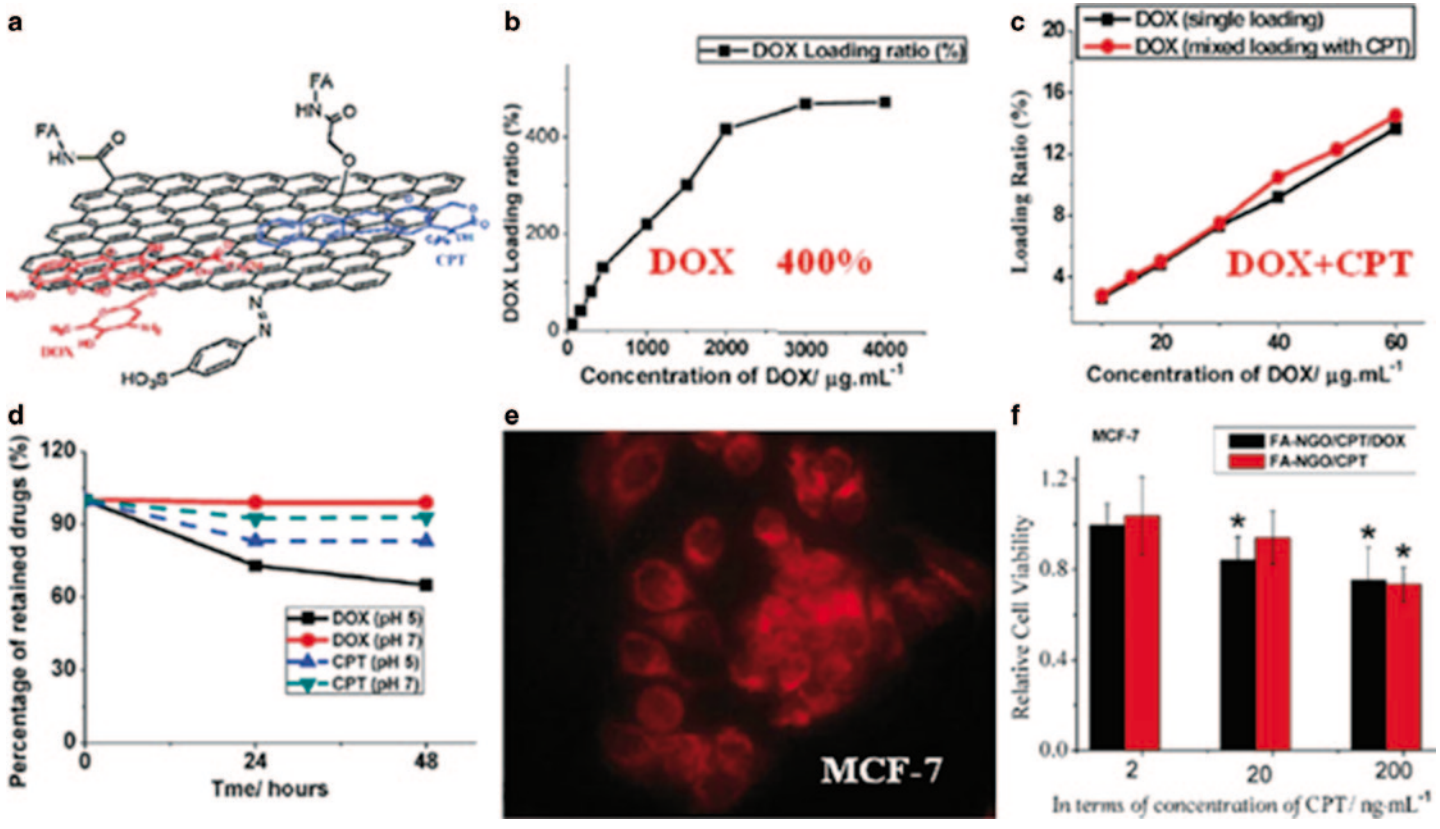

Fig. 8.1 **a** DOX and CPT loaded onto FA–NGO. **b** The loading ratio of DOX to FA–NGO versus the concentration of DOX. **c** The loading ratio of DOX to FA–NGO versus concentration of DOX in a mixture of DOX and CPT (concentration of CPT 100 μgmL^{-1}). **d** The release of DOX and CPT from FA–NGO at pH 5 and 7, respectively. **e** Image of MCF-7 cells incubated with FA–NGO/Rho B for 2 h. **f** Relative cell viability of MCF-7 treated with FA–NGO/CPT and FA–NGO/DOX/CPT. *DOX* doxorubicin, CPT camptothecin, *FA–NGO* folic acid–nanoscale graphene oxide. (Adapted with permission from Ref. [9]. Copyright 2010 Wiley-VCH Verlag GmbH & Co. KGaA, Weinheim)

apy can avoid severe side effects of chemical drugs to normal cells and tissues due to its targeting effect to specific cancer cells [16]. In order to help a piece of DNA to successfully reach specific cancer cells, suitable gene vectors with low toxicity, cell or tissue specificity, and good transfection efficiency are highly demanded [17].

Zhang group and Liu group, respectively, investigated gene delivery by GO modified with PEI to supply positive charges and to allow the condensation of the negatively charged plasmid DNA (pDNA) onto GO surface by electrostatic interaction [18, 19]. Zhang group conjugated GO with PEI via amide bond, and utilized this GO–PEI to deliver pDNA. According to the authors, PEI not only improved GO's physiological stability but also facilitated the condensation of pDNA and GO (ratio of PEI–GO to pDNA > 1:1). As the in vitro study suggested, high DNA transfection efficiency with GO–PEI in HeLa cells was achieved even in the presence of 10% phosphate-buffered saline (PBS), which largely improved the degradation of PEI's transfection efficiency when grafted to other systems [18]. Liu and colleagues further demonstrated that GO could significantly improve the transfection efficiency of PEI with low molecular weight (1.2 K) and decrease the cytotoxicity of large PEI (10 K) [19]. In addition, Kim et al. grafted a low-molecular weight branched PEI (BPEI) onto GO and applied this system to deliver genes into HeLa and PC-3 cells. BPEI–GO exhibited high cell viability and improved gene transfection efficiency, owing to the multivalent effect of BPEI conjugated to GO and the formation of stable polyelectrolyte complexes of BPEI–GO and pDNA [20].

In order to overcome multiple drug resistance (MDR) of cancer cells, Zhang et al. employed PEI-grafted GO nanocarrier for sequential delivery of Bcl-2-targeted small interfering ribonucleic acid (siRNA) and DOX. Because Bcl-2 protein is one of the main antiapoptotic defense proteins, Bcl-2-targeted siRNA was utilized to reduce the Bcl-2 protein expression level in cancer cells and thus to overcome the MDR of cancer cells [21]. The sequential delivery of siRNA and DOX with PEI–GO showed remarkedly enhanced chemotherapy efficacy due to strong synergistic effect of DOX and Bcl-2-targeted siRNA, which significantly inhibited Bcl-2 expression [14]. Similarly, Bao et al. developed positively charged chitosan (CS)-modified GO (CS-GO) for the co-delivery of (pRL-CMV) genes and anticancer drug CPT into HeLa cells [22].

The photothermal property of GO has been integrated to gene delivery, in addition to drug delivery. Feng et al. fabricated NGO with both PEG and PEI (NGO–PEG–PEI) and demonstrated its gene delivery application with excellent physiological stability, superior gene transfection efficiency, and low cytotoxicity [23]. In addition, they found that photothermally induced local heating accelerated intracellular trafficking of nano-vectors, resulting in remarkably enhanced plasmid DNA transfection efficiency under NIR laser irradiation at a low power density.

8.2.3 GO for Protein Delivery

Proteins play important roles in physiological activities of cells and functions of living organisms by regulating the expression of gene and cellular signaling pathways.

Protein-based biotherapy has significant advantages over traditional chemotherapy, such as high specificity to cell functions, and very low side effects and immune responses [24]. However, proteins have difficulties to penetrate the cell membrane, requiring suitable delivery vehicles to facilitate their entry into cells [6].

Shen et al. delivered proteins into cells with PEG–GO [24]. In their study, proteins were loaded onto GO–PEG via non-covalent interaction and then efficiently delivered into cytoplasm with the protection of GO–PEG. More importantly, this work demonstrated that after delivered into cells by GO, the proteins retained their functions to determine cell fate. The ribonuclease A (RNase A) delivered by GO–PEG led to cell death while protein kinase A (PKA)-induced cell growth.

8.2.4 GO for Photothermal Therapy

Photothermal therapy (PTT), as a minimally invasive treatment, employs hyperthermia to kill cancer cells. In this treatment, NIR-absorbing photothermal agents are first delivered to tumor site and then irradiated with an NIR laser. The NIR light can safely penetrate tissues as deep as several millimeters and was converted to heat by PTT agents to generate localized hyperthermia and destroy nearby cells [25].

GO itself is very suitable for PTT because of its strong NIR absorption, excellent photo-stability, and high photothermal conversion efficiency. Liu group [25] demonstrated GO's potential for efficient in vivo PTT without obvious side effects. In this work, GO was modified with amine-terminated six-arm-branched PEG to increase its biocompatibility. They have demonstrated that the branched PEG facilitated the exfoliation of GO sheets while broke the sheets into smaller ones (< 50 nm), and thus enhanced its stability and biocompatibility [11]. The PEGylated GO exhibits highly efficient tumor passive targeting and relatively low retention in reticuloendothelial systems (RES) due to its unique 2D structure, small size, and biocompatible PEG coating. Then, an NIR laser of 808 nm was utilized to irradiate GO (intravenous administration) for in vivo photothermal therapy, leading to ultraefficient tumor ablation, even with low-power NIR laser irradiation suitable for clinical use (Fig. 8.2). Dai group [26] developed nano-sized, reduced GO (nano-rGO) sheets and stabilized this GO with PEGylated lipids though non-covalent adsorption. Interestingly, they found that the nano-rGO shown sixfold higher NIR absorption than the nonreduced, covalently PEGylated nano-GO due to the stronger absorption of rGO in the visible and NIR region. In addition, the tumor treated with nano-rGO still showed 100 % tumor elimination efficacy [27], even under low power density laser irradiation (0.15 W/cm^2, 808 nm, 5 min), which is an order of magnitude lower than that usually applied for many other nanomaterials in vivo tumor ablation. This work also discussed how surface chemistry and size of GO affect the in vivo performance of graphene. As the results showed, GO with smaller size and more PEG coating appears to be a more effective agent for in vivo PTT ablation of cancers.

GO acts as a carrier for drug delivery and can also serve as a platform to combine other therapeutic modalities for improved PTT anticancer efficacy. For example,

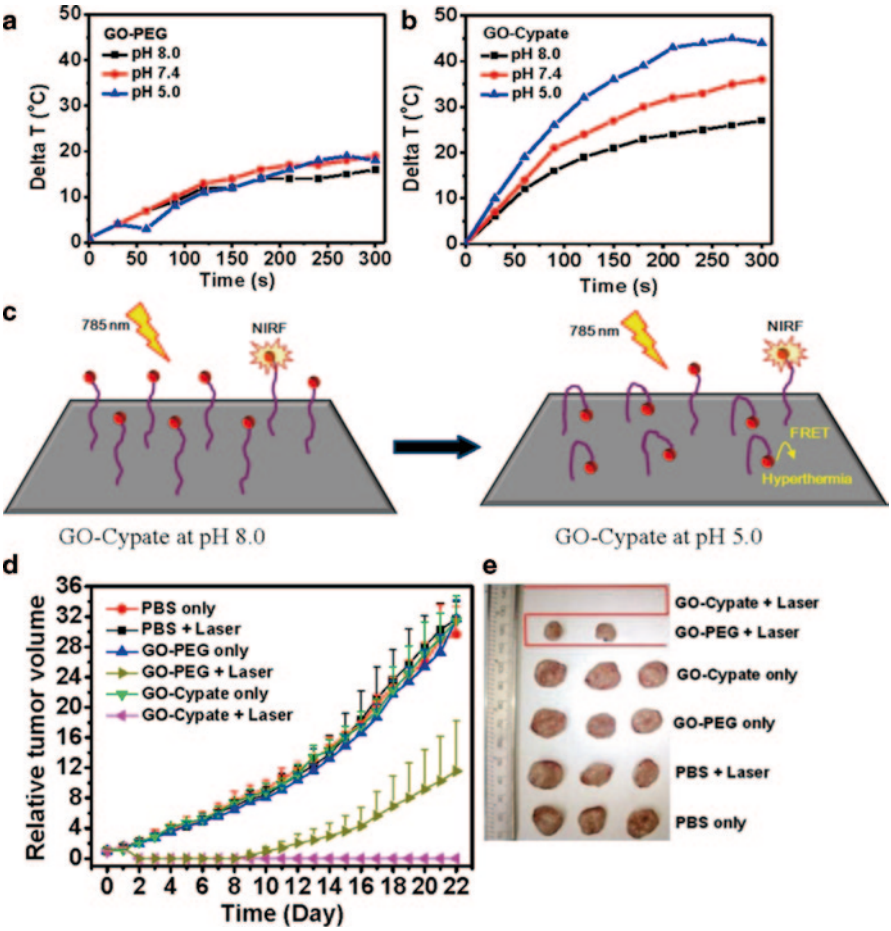

Fig. 8.2 Photothermal effects of GO–PEG (**a**) and GO–Cypate (**b**) in the buffers at various pH within 5 min of photoirradiation, respectively. **c** Conformation illustration of GO–Cypate at different pH and thereof FRET between GO and Cypate. **d** Tumor growth inhibition profiles of the mice bearing 4T1 tumor injected with GO–Cypate and GO–PEG at the same concentration of GO, respectively, followed by 785 nm PTT treatments (5 min, 1.0 W/cm^2) at 24 h post injection. **e** Photos of the tumors extracted from the mice at the end of the PTT therapy (day 22). *GO* graphene oxide, *PEG* polyethylene glycol, *PBS* phosphate-buffered saline, *FRET* fluorescence resonance energy transfer. (Adapted with permission from Ref. [28] Copyright 2014 Wiley-VCH Verlag GmbH & Co. KGaA, Weinheim)

photosensitizers, CuS nanoparticles, and gold nanostructures have been conjugated with GO for the PTT therapy, leading to superior therapeutic efficacy compared to bare GO-induced PTT treatment. Guo et al. [28] covalently conjugated GO with Cypate, an NIR fluorescence imaging agent approved for clinical use by Federal Drug Administration. They demonstrated that GO could increase the dispersibility, half-life in circulation and the targeting ability of Cypate. Upon the irradiation of NIR light at 785 nm (1.5 W/cm^2), a rapid increase of temperature in a GO–Cypate

solution was observed, and GO was also proved to prevent the light-induced decomposition of Cypate (Fig. 8.2). In addition, GO–Cypate at pH 5.0 exhibited much higher temperature increase under photo-irradiation than that at pH 7.4 and 8.0. This phenomenon was attributed to more efficient fluorescence resonance energy transfer (FRET) from Cypate to GO, based on the facts of weakened fluorescence intensity and enhanced PTT ability, because Cypate molecules might form severe aggregation on GO surface in acidic environment. GO was also conjugated with metal nanoparticles to obtain a synergistically improved photothermal effect. El-Shall et al. [29] conjugated laser-reduced GO with Au nanomaterials of different size and shape, and successfully adjusted the photothermal effects by controlling the shape and size of the gold nanomaterials. As the authors illustrated, decrease in size of the gold nanostructures led to a prominent increase in the heating effciency, and composites of ultrasmall gold nanoparticles of 2–4 nm anchoring onto graphene surface generated a highly efficient photothermal effects. Liu group [30] decorated GO with both iron oxide nanoparticles (IONPs) and gold nanoparticles to construct GO–IONP–Au nanocomposites. Compared to PEGylated GO used in their earlier studies, GO–IONP–Au nanocomposites significantly enhanced optical absorbance in the NIR region, and remarkably enhanced photothermal cancer ablation effect in the in vitro and in vivo experiments.

8.2.5 GO for Photodynamic Therapy

Photodynamic therapy (PDT) has emerged as a promising cancer treatment since it can selectively destroy the diseased tissues after the uptake of photo sensitizers (PSs) by cancer cells followed by irradiation [31]. PDT involves the systemic, local, or topical administration of photosensitizers, then light irradiation with appropriate wavelength and dosage, and subsequent production of reactive singlet oxygen ($^1O_2$) species inducing cytotoxic effect [32].

GO offers great promise in PDT applications. In 2011, Cui group first studied the graphene-based carriers on the controlled loading and targeted delivery of chlorine-6 (Ce6), a promising photosensitizer with a high sensitizing efficacy [33]. In this experiment, FA molecules were covalently conjugated with GO for specific targeting to the cells with folate receptors, and Ce6 was loaded onto GO via π–π staking. As the results indicated, GO efficiently transported Ce6 to tumor cells, resulting in significant increase of the Ce6 accumulation in tumor cells, and thus remarkable photodynamic efficacy on MGC803 cells upon irradiation. Chen group [34] demonstrated tumor ablation by PDT modality with novel nanocomposites of GO–PEG–HPPH, in which graphene serves as the carrier and 2-(1-hexyloxyethyl)-2-devinyl pyropheophorbide-alpha (HPPH) as the photosensitizer to treat xenograft tumors with PDT. GO–PEG–HPPH revealed higher tumor uptake than free HPPH after intravenous administration, resulting in significant tumor destruction upon the irradiation of 671 nm laser with low power (75 mW/cm^2). These results demonstrated that graphene can improve PDT efficacy as a carrier of PDT agents and significantly increase long-term survival of tumor-bearing mice following the treatment.

In addition, usGO, or GQD, has been illustrated as a photodynamic agent. Markovic et al. showed that electrochemically produced GQD generated reactive oxygen species, including singlet oxygen when irradiated with blue light (470 nm, 1 W), and then killed U251 human glioma cells by causing oxidative stress [35]. Similarly, Ge et al. reported a new PDT agent based on GQDs derived from hydrothermal treatment of polythiophene [36]. This GQD sample displayed an extremely high quantum yield of ~1.3 for $^1O_2$ generating, via a multistate sensitization process of energy transfer from the excited triplet state (T_1) and the excited singlet state (S_1) to the ground-state oxygen ($^3O_2$). Also, the in vitro and in vivo imaging of GQD was demonstrated in this study.

8.2.6 GO for Multimodal Therapy

While conventional cancer therapy techniques often fail to completely eradicate the tumor, there is a trend of combinational therapy with several therapeutic agents or multimodal therapy leading to synergistic effect. Owing to its high surface area and easy surface functionalization, GO is often used as a multitasking nanocarrier for multiple anticancer drugs and NIR dyes to achieve photothermal–photodunamic, chemo-photodynamic, or chemo-photothermal synergistic therapies.

Tae group [37] integrated PTT and PDT agents into a GO system for advanced in vivo cancer therapy by loading hydrophilic photosensitizer (methylene blue, MB) on NGO. The NGO efficiently localized in cancer cells with photosensitizer and caused complete ablation of tumor under exposure to NIR light, due to the combination of PDT induced by MB and subsequent photothermal therapy from NGO. This PDT–PTT combined therapy utilized smaller GO dose (10 mg/kg) and short irradiation time (3 min) compared to PTT alone (20 mg/kg, 5 min) [25], indicating synergistic effect of dual phototherapy. In another work from Liu group [38], Ce6 was loaded on GO–PEG via π–π stacking (GO–PEG–Ce6) showed a remarkably improved cancer cell photodynamic destruction effect. Interestingly, the photothermal effect of GO can further enhance the PDT effcacy against cancer cells, because NIR light-induced local heating increased the cellular uptake of GO–PEG–Ce6 although GO slightly inhibit the singlet oxygen generation of Ce6. In this way, complete tumor elimination with mild local heating at a low power density (0.3 W/cm^2) of the NIR laser was achieved.

Similarly, the photothermal effect of GO has been demonstrated to improve the chemotherapy of tumor. Wang and colleagues [39] prepared a novel nanostructure NGO–AuNRs with gold nanorods (AuNRs) encapsulated in NGO shells through electrostatic self-assembly between the negatively charged NGO and the positively charged AuNRs. Adipic acid dihydrazide (ADH)-modified HA (HA-ADH) was conjugated onto the surface of NGO–AuNRs to increase the targeting to hepatoma Huh-7 cells. DOX was then loaded on NGO–AuNRs composites by π–π stacking as a model anticancer drug. Compared to bare AuNRs and NGO, the HA-conjugated NGO-enwrapped AuNR nanocomposites (NGOHA–AuNRs) yielded higher photothermal effciency. Due to the superior photothermal promotion of NGOHA–

AuNRs to the release of DOX, NGOHA–AuNRs–DOX performed 1.5-fold and 4-fold higher targeted cell death rates than single chemotherapy and photothermal therapy, respectively.

The Kim group combined gene therapy and photothermal therapy together with the help of GO [40]. They developed nano-sized, PEG–BPEI–rGO nanocomposite as a potential PTT agent, which combined rGO sheets with BPEI and PEG through covalent conjugation. The transfection efficiency of PEG–BPEI–rGO with laser irradiation was increased approximately two- to threefold than the transfection without irradiation. As the authors demonstrated, endosomal membrane was ruptured due to the local increase in temperature caused by NIR irradiation, and then the PEG–BPEI–rGO complex escaped from endosomal, which induced high gene transfection.

Zhang et al. explored GO as an adjuvant for immune therapy [41], by using a usGO–Au composite through in situ growth of gold nanoparticles on usGO sheets. Excellent adsorbing capacity of GO could improve the binding capacity of usGO-supported AuNPs to ovalbumin (OVA) proteins. In vivo study revealed that usGO–Au@OVA could promote robust OVA-specific antibody response, $CD4^+$ and $CD8^+$ T cells proliferation, and the secretion of tumor necrosis factor (TNF)-α and interferon (IFN)-γ.

8.3 Bioimagimg

Over the past several years, graphene and its derivatives, especially GO, have displayed appealing prospects in bioimaging field. Owing to their versatile surface modification, graphene and GO have been explored with various molecular imaging techniques, including magnetic resonance imaging (MRI), positron emission tomography (PET) imaging, photoacoustic, and fluorescence imaging. Besides, due to their high drug-loading capability and photothermal effects, integration of diagnostics and therapies into one graphene platform, namely theranostics, has recently drawn increasing attention in the treatment of diseases.

The imaging ability of GO is mostly achieved by conjugation to one or multiple imaging components. Therefore, a linkage molecule with additional chemical reaction sites is required for further functional modifications, and the linkers are normally among macromolecules, such as PEG [42], and poly(amido amine) (PAMAM) [43]. Moreover, these macromolecules can also enhance the biocompatibility and stability of GO in physiological solutions. Figure 8.3 shows the common structure of GO composites for imaging or/and therapy.

8.3.1 Optical Imaging

The technique of fluorescence imaging has been widely studied in tracking and monitoring live cells with graphene and its derivatives, through decorating GO or

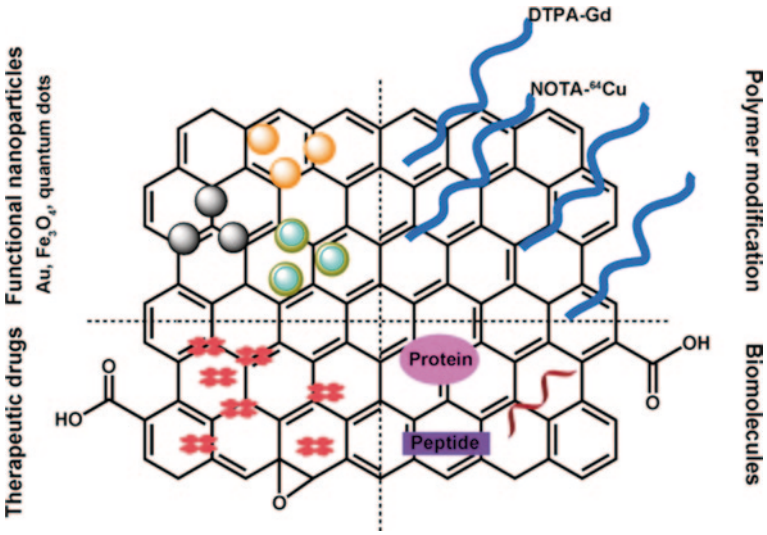

Fig. 8.3 Surface modification of graphene and graphene oxide for bioimaging and therapy. Different functional moieties (*polymers, nanoparticles, anticancer drugs, biomolecules*) could be anchored for specific purposes. *NOTA* 1,4,7-triazcyclonoane-1,4,7-triacetic acid, *DTPA* diethylene triamine pentaacetic acid

rGO with highly fluorescent inorganic fluorophores or organic dyes [43, 44]. To avoid the fluorescence quenching by GO, it is necessary to shield GO from fluorescent component with long molecular linkers, such as PEG [45], BSA [46], or an SiO_2 shell [47]. In addition, passivating the surface reactive sites of GO by using alkylamines [48] or branched PEI [20] has also been attempted.

Peng et al. linked fluorescein with PEGylated GO and used this fluorescent GO as an intracellular fluorescence imaging probe [45]. Fluorescein-modified GO exhibited excellent green fluorescence when incubated with HeLa cells for 6 h, while GO as the control group showed no fluorescence. Similarly, Hu et al. decorated quantum dots (CdSe/ZnS) with polypeptide-modified rGO through physical adsorption. The surface of quantum dots was covered with tri-*n*-octylphosphine oxdie (TOPO) and 11-mercaptoundecanoic acid (MUA), which served as a spacer to prevent fluorescence quenching. In this preliminary experiment, significant fluorescence can be monitored when two kinds of QDs–rGO with different color were subcutaneously injected into nude mice. Moreover, owing to the strong NIR absorbance of rGO, a QDs–rGO system can kill cancer cells through photothermal effect at the same time [49]. According to the authors, the fluorescence of QDs provided indicative information for the heat dosage and the treatment process, leading to subsequent cancer ablation with minimized damages to healthy organs and tissues. In addition, precise monitoring of the tumor change can be obtained during photothermal therapy.

Wang et al. covalently grafted upconversion nanoparticles ($Tm^{3+}/Er^{3+}/Yb^{3+}$ co-doped $NaYF_4$) onto PEGylated GO and then loaded a photosensitizer (phthalocyanine) to build a multifunctional theranostic platform for in vivo imaging and combination of PDT/PTT [50]. In this study, strong upconversion luminescence imaging

of a white Kunming mouse was monitored and further applied to demonstrate the enhanced efficacy of combinational therapy of PDT/PTT compared to PDT or PTT alone. The synergistic effect probably was ascribed to the photothermal property of GO, which not only heated the cancer cells but also enhanced the delivery of PDT agents to the cancer cells.

As a representative fluorescence probe in the family of graphene, GQD are small graphene fragments with size range below 10 nm. Owing to its good biocompatibility and excellent optical properties, GQD has been explored widely for bioimaging applications based on its size-related fluorescence [51]. Zhang et al. employed a yellow-light-emitted GQD to simultaneously monitor three kinds of stem cells, neurospheres cells (NSCs), pancreas progenitor cells (PPCs), and cardiac progenitor cells (CPCs). According to their study, GQD mainly retained in cytoplasmic area and did not affect the viability, proliferation, or differentiation of the stem cells [52]. Nurunnabi et al. prepared a series of GQD samples with different colors by regulating the reaction temperature during oxidative cutting of carbon fibers. These GQDs possessed varied emission ranging from 460 to 805 nm in wavelength, due to various oxygen contents defining the band gaps. In addition, GQDs were intravenously injected into nude mice to illustrate their attractiveness as new noninvasive imaging agents [53].

8.3.2 MR Imaging

MRI is a powerful noninvasive imaging technique in clinical diagnosis. Among various MRI contrast agents which provide more precise information in pathological tissues, superparamagnetic Fe_3O_4 nanoparticles are most commonly used in T_2-weighted MRI. Chen et al. conjugated Fe_3O_4 nanoparticles onto GO and demonstrated that the Fe_3O_4–GO composites significantly improved T_2 relaxivity and thus enhanced the cellular MRI effect, owing to the formation of aggregates of the Fe_3O_4 nanoparticles on the GO sheets. In another study, Yang et al. in situ synthesized Fe_3O_4–rGO nanocomposites through hydrothermal reaction and expanded the application of GO/Fe_3O_4 nanocomposites not only for imaging but also for cancer therapy. Due to the strong NIR optical absorbance and T_2 MRI of the nanocomposites, rGO–IONP–PEG exhibited remarkable photoacoustic imaging and MRI effect and photothermal therapy efficacy [54].

To obtain T_1-enhanced MRI signal, Zhang et al. conjugated Gd–diethylene triamine pentaacetic acid (DTPA) to PEGylated GO and demonstrated the significant improvement of T_1 MRI relaxivity for GO–DTPA–Gd and cellular MRI with effective internalization of the composites into cells [55]. In a recent report, Yang et al. prepared Gd–DTPA grafted NGO (Gd–NGO) and then loaded with Let-7 g miRNA and anticancer drug epirubicin (EPI). This system (Gd–NGO) showed combined chemo- and gene therapy effect to malignant glioblastoma cells. Moreover, Gd–NGO was utilized to monitor the location and extent of blood–brain barrier (BBB) opening, which was induced by focused ultrasound (FUS) in the presence of circulating microbubbles. The in vivo experiment demonstrated that more intensive signals in the region of interest can be detected by using Gd–NGO [56].

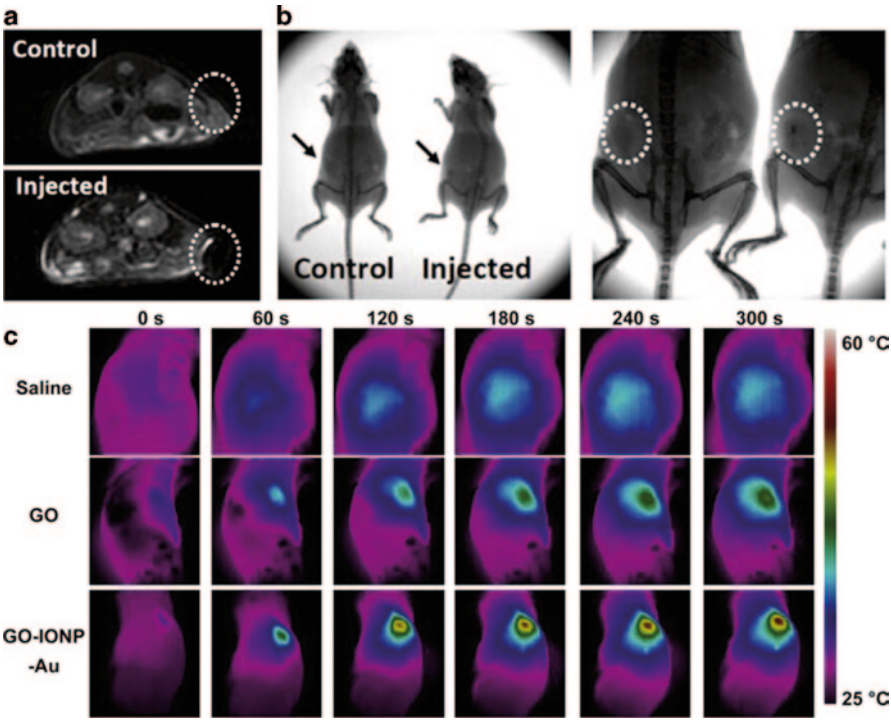

Fig. 8.4 In vivo dual-modal MRI/X-ray imaging and PTT. **a** T_2-weighted MR images of 4T1 tumor-bearing mice before (*top*) and after (*bottom*) intratumoral injection of GO–IONP–Au. **b** X-ray images of tumor-bearing mice before (*left*) and after (*right*) intratumoral injection of GO–IONP–Au. Tumors are highlighted by *black arrows* or *white circles*. **c** IR thermal images of tumor-bearing mice injected with *saline*, GO or GO–IONP–Au under laser irradiation (808 nm, 0.75 W/cm^2). *GO–IONP* graphene oxide–iron oxide nanoparticle. (Adapted with permission from Ref. [30]. Copyright 2013 Elsevier B.V.)

Since each molecular imaging tool has its own merits and limitations, the integration of multiple techniques into a single platform can provide distinct and synergistic advantages. Particularly, GO is a suitable candidate for such a platform due to its unique physicochemical properties, such as large surface area and versatile functionalization. Shi et al. decorated GO with iron oxide and gold nanoparticles and demonstrated synergistic imaging through in vivo experiment (Fig. 8.4). In addition to enhanced photothermal cancer ablation, this system was used for enhanced MRI and X-ray dual-modal imaging by taking the advantage of iron oxide and gold nanoparticles [30].

8.3.3 Photoacoustic Imaging

As a newly emerged imaging technique, photoacoustic imaging has attracted ever increasing interest in recent years because it offers significant increase in imaging

depth in diagnosis. Sheng et al. developed a simple method to fabricate rGO by using bovine serum albumin (BSA) as a reductant and a stabilizer. Due to the strong NIR absorbance of BSA-functionalized nano-rGO, it was used for in vivo photoacoustic imaging as well as photothermal therapy, which are both triggered by the transformation between light and heat [57].

8.3.4 PET Imaging

Initially developed in the mid-1970s, PET imaging is another noninvasive imaging technique that provides a three-dimensional (3D) image in the body. It is capable of quantitatively measuring the radioisotope concentrations in vivo with excellent tissue penetration [58]. Shi et al. designed a PET imaging agent based on rGO conjugated with 1,4,7-triazcyclonoane-1,4,7-triacetic acid (NOTA), which was used as an effective chelator to ^{64}Cu for radiolabeled PET imaging. Particularly, TRC105, a human/murine chimeric immunoglobulin G (IgG)1 monoclonal antibody, was conjugated to rGO as a tumor vasculature-targeting ligand to CD105, which serves as an ideal vascular target expressed on proliferating tumor endothelial cells. Tumor vasculature targeting is important since it is more instantly accessible upon intravenous injection. Moreover, new blood vessel formation is a critical process in tumor growth and metastasis. Through the noninvasive PET imaging technique, the specific targeting of ^{64}Cu–NOTA–rGO–TRC105 to CD105 in 4T1 murine breast tumors model was demonstrated, suggesting rGO conjugates as promising candidates for in vivo tumor vasculature targeting [59].

8.3.5 Raman Imaging

Raman spectroscopy is another powerful technique for biological imaging, as it provides a high signal-to-noise ratio and can distinguish different fingerprints of the Raman probes in a nondestructive way. It is well known that metal nanoparticles, especially Au and Ag nanoparticles, can significantly improve the Raman signal of probe molecules [60–62], that is, surface-enhanced Raman scattering (SERS) effect. Based on the distinctive Raman spectra of GO, researchers have decorated Au or Ag nanoparticles onto GO for detection or cellular imaging by using this SERS technique. Au/GO hybrids was employed as a Raman probe to investigate the internalization mechanism of GO, which was found to be a clathrin-mediated, energy-dependent endocytosis [15].

In another study, Wang et al. built a nanocomposite by anchoring gold nanoclusters (GNCs) on rGO, and further utilized it as a Raman spectroscopy probe to investigate the interactions between the GNC–rGO nanocomposites and proteins and DNA. Their study suggested that the presence of GNC–rGO induced DNA chain disorder and affected the protein α helices without disturbing β folding [63].

8.4 Graphene for Biological Sensors

8.4.1 Graphene-based Electrochemical Sensors

Graphene has been extensively studied to fabricate electrodes for electrochemical sensors, due to its excellent absorbing ability, efficient charge transfer, large electrochemical potential window, and tunable chemical and electrical properties. In order to gain facile fabrication, rGO, rather than pristine graphene or GO, was generally applied due to its abundant functional groups and high electrochemical activity [2].

Interestingly, benefited from its high potential (~2.5 V), rGO shows significant catalytic activity toward some small enzymatic products such as H_2O_2 and nicotinamide adenine dinucleotide (NADH). In addition, the large surface area of GO facilitates target loading, making it attractive for enzyme-based sensors. For example, hemoglobin embedded in an rGO-CS film can facilitate a H_2O_2 sensor with a limit of detection (LOD) of 0.51 uM [64]. Furthermore, with the help of horseradish peroxidase (HRP) to hydrolyze H_2O_2, and sodium dodecyl benzene sulfonate to improve the enzyme loading because of intercalation, a lower LOD of 0.1 uM was achieved by Zeng and coworkers [65].

Glucose oxidase (GOD) can specifically recognize glucose which is a significant element for the diagnosis of diabetes, so it can be incorporated into graphene-based electrodes for the electrochemical detection of glucose. Kang et al. showed a GOD–rGO–CS electrode with high sensitivity (0.02 mM of LOD) [66]; while Alwarappan et al. constructed a conducting porous matrix with GOD, rGO, and polypyrrole (ppy), and improved the LOD to 3 uM [67]. In addition, decoration of in situ-grown metal nanoparticles on rGO can further lower the LOD to 0.6 uM [68], of which the high performance was attributed to the facts that the highly conductive nature of the metal nanoparticles facilitates rapid charge transfer on rGO sheets.

Thanks to the strong π–π stacking and electrostatic attraction between GO and nucleobases, development of DNA sensors based on rGO are also realized. Huang et al. applied GO with abundant carboxylic groups for highly sensitive detection of guanine (50 nM) and adenine (25 nM) [69]. Du et al. decorated an rGO electrode with AuNPs through potentiostatic electrodeposition for the detection of single-stranded DNA (ssDNA) [70]. Furthermore, they demonstrated that the oxidation signal of thymine can be distinguished from that of adenine, making the detection of single-base mutation possible without any labeling or probe DNA. In a work of Lim et al., double-stranded DNA (dsDNA) could be differentiated from ssDNA with a graphene-based SiC electrode, which is impossible for conventional electrodes because of their limited electrochmemical potential window [71]. In addition, GO-modified electrode was introduced to detect DNA hybridization, through the guanine oxidation signal from the target ssDNA molecules without guanine base [72].

Graphene-based electrochemical sensors have been used to detect various protein markers, when an antibody was applied. Su et al. used the interaction between alpha fetoprotein (AFP) and anti-AFP antibody to partially block HRP reducing H_2O_2, with an LOD of 0.7 ng/mL [73]. The authors applied HRP and electropolymerized

thionine (TH) films, which was constructed with GO-CS through layer-by-layer assembly, to mediate the electron transfer from H_2O_2 to the electrode. On the other hand, Wei et al. directly embedded TH in rGO film through π–π stacking and then covalently cross-linked AFP antibody with TH. With intimate interaction of rGO and TH for efficient electron transfer, as well as high loading of TH and AFP antibody molecules on the rGO film, they achieved a much lower LOD of 5.77 pg/mL, and successfully applied this sensor to AFP detection in serum [74].

A highly sensitive and selective dopamine sensor (0.01 uM) was demonstrated by Hou et al. [75]. In this report, ethylenediamine triacetic acid (EDTA)-modified graphene (EDTA-GO) was chosen to fabricate a glass carbon electrode for several reasons. (1) EDTA-GO greatly enhanced the electrochemical activity in physiological solutions and effectively increased the surface area on electrode, (2) EDTA groups could concentrate DA from the solution, (3) EDTA groups linked to GO surface promoted the electron transfer, and (4) carboxylic groups of EDTA could block the diffusion of ascorbic acid and thus avoid its interference. Furthermore, Tan et al. [76] illustrated that β-cyclodextrin could greatly enhance the electron transfer for the rGO electrode, obtaining a lower LOD of 5 nM for the detection of dopamine.

8.4.2 Graphene-based Electronic Sensors

Graphene-based electronic sensors, normally considered as field effect transistors (FETs), are expected to display a high signal-to-noise ratio for several reasons. First, graphene and GO show high carrier mobility and carrier density, as well as low intrinsic noises; second, graphene's planar structure enables its extreme exposure to the environmental variation and thus highly sensitive conductance of graphene; and third, the gate voltage of graphene can be manipulated with various doping for different charge transfer. In addition, graphene provides a large detection area for cell detection and allows simultaneous optical observation during electrical measurement. Therefore, graphene and its derivatives have been applied to various electronic sensors, providing vast new possibilities.

A graphene-based electronic sensor for the detection of glucose and glutamate was illustrated by Chen et al., with an LOD of 0.1 mM and 5 μM [77]. The detection through increased conductance of graphene film was mediated by H_2O_2 (p-dopant), which was generated by specific enzymes, GOD, and glutamate dehydrogenase, respectively. Similarly, proteins bearing charges or dipoles can bind onto the surface of graphene via π–π interaction, and thus can be detected through the doping effect. Ohno et al. developed a pristine graphene device for the detection of BSA with an LOD of 0.3 nM, based on the nonspecific adsorption of graphene to BSA molecules, which is negatively charged under physiological condition [78]. However, the adsorption lacks recognition to targets, missing specificity in detection.

In order to offer an electronic immunoglobulin E (IgE) sensor with specificity, Ohno et al. modified the graphene surface of the sensor with IgE-specific aptamers, observing dramatic decrease in the conductance of p-type graphene due to field

effect when positively charged substances interacted with graphene [79]. In another work, Mao et al. assembled AuNPs and anti-IgG antibody on an rGO film, and they employed a blocking buffer to minimize nonspecific binding, obtaining an LOD of 13 pM. Similarly, BSA was used to improve the specificity of a graphene immunosensor for the detection of prostate-specific antigen (PSA) using rGO sheets, leading to an immunoglobulin G electronic sensor with wide detection range (0.1–100 ng/mL) [80].

Mohanty et al. reported a DNA sensor made of GO sheets, which was modified with probe ssDNA via simple π–π stacking. When hybridization of the target DNA occurred, the conductance of GO sheets increased owing to p-doping effect, as the author determined. Since the measurement of conductance was performed under dry condition, field effect did not fit the situation because DNA molecules contained no charges [81]. On the contrast, Dong et al. developed an electronic DNA sensor with chemical vapor deposited (CVD)-grown graphene and suggested that the detection of hybridization of DAN in solution was based on n-doping effect [82]. In addition, this sensor could detect single-base mismatch of the target ssDNA with an LOD of 10 fM.

Cells can intimately interact with graphene film, without damage to the local curvature. Therefore, graphene-based electronic sensors have been applied to the detection of cells due to the tight and homogeneous interaction between cells and graphene, as well as sensitive electronic properties of graphene. Cohen-Karni et al. demonstrated a graphene FET for the detection of cardiomyocyte cell bioactivity (Fig. 8.5) [83]. It was the field effect that triggered the device response, because electrical potential changed at the nano-interface between the cell and the FET due to the ionic current flows through the membrane ion channels. Compared to conventional metallic microelectrodes and a silicon nanowire FET, the graphene FET showed comparable sensitivity and signal-to-noise ratio. He et al. fabricated a centimeter-long and a micrometer-wide ultrathin rGO film through microfluidic patterning and coupled the rGO film with neuroendocrine PC-12 cells (Fig. 8.5) [84]. This rGO FET could detect rapid vesicular secretion of hormone catecholamine of PC-12 cells due to membrane depolarization, because catecholamine molecules released from the cells interacted with rGO sheets through p–p interaction, and increased p-type rGO conductance via p-doping. In addition, the authors claimed that microfluidic patterning technique enabled flexible sensors for curved targets, for example, organs. In addition, Kempaiah et al. [85] coupled rGO coating on a yeast cell, and monitored in real time the dynamic mechanical response of a yeast cell to osmotic stresses or heat shock based on the change in the electrical conductance of the rGO layer.

8.4.3 Optical Sensors

Graphene and its derivatives possess strong absorption over a wide range from ultraviolet to IR region, showing highly efficient quenching effect to fluorescence. In

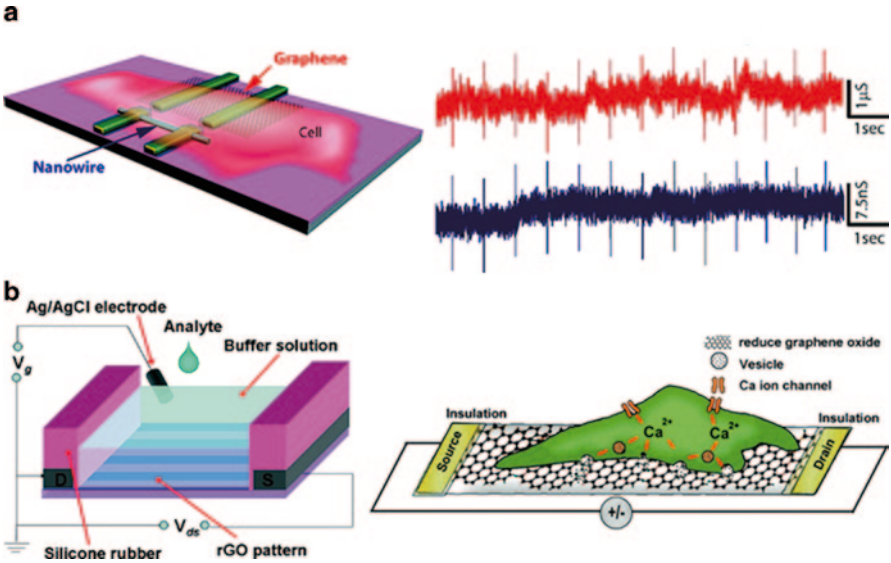

Fig. 8.5 **a** Graphene and nanowire transistors for cellular interfaces and electrical recording chip, from which the signals from cardiomyocytes was recorded at different applied water gate potentials. (Adapted with permission from Ref. [83]. Copyright 2010 American Chemical Society). **b** The interface between a PC-12 cell and rGO FET. *rGO* reduced grphene oxide. (Adapted with permission from Ref. [84]. Copyright 2010 American Chemical Society)

addition, the defects, mostly oxygen-containing functional groups, on graphene and GO surface restrict free π electrons, and thus create a wide range of local energy gaps due to various sizes of sp^2 domain. Therefore, GO was extensively explored as optical sensors based on FRET. Generally, a GO-based FRET sensor contains three components, including GO flakes as quencher, a reporter as fluorescence donor, and a recognition probe linked to the reporter. The detection of target molecules relies on that the probe molecules associate with the targets and then induces turn-on fluorescence due to the release of fluorescent reporter from the GO surface.

Graphene can selectively adsorb ssDNA over dsDNA, due to strong π–π interaction between nucleosides and graphene. Taking advantage of protection of ssDNA from enzymatic cleavage by GO, Tang et al. designed a DNA optical sensor based on a ssDNA and DNAse I, obtaining an LOD of nanometer range [86]. Furthermore, the authors showed that ssDNA was intact to DNAase when adsrobed on the GO surface. This design strategy of selectively interacting with ssDNA has also been applied to build other DNA sensors [87, 88]. In addition, Huang et al. developed a graphene-based DNA sensor for simultaneous detection of multiple ssDNAs, through distinctly colored probes linked with different DNA targets. As the study revealed, the interference between different targets was negligible, and the detection limit reached as low as 100 pM [89].

Using highly specific binding of aptamers, protein sensors have also been developed based on similar designs. Lu et al. demonstrated graphene-derived sensors

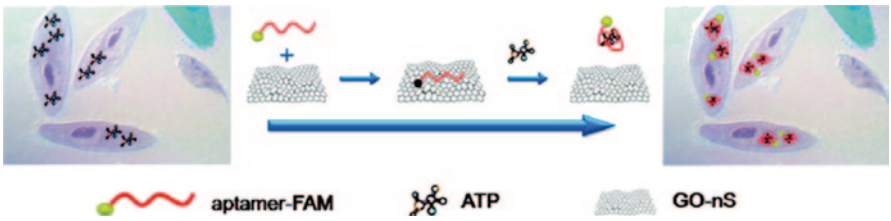

Fig. 8.6 Illustration of in situ molecular probing in living cells by using an aptamer-carboxyfluorescein (FAM)/graphene oxide nanosheet (GO-nS) nanocomplex. *ATP* adenosine triphosphate. (Adapted with permission from Ref. [93]. Copyright 2010 American Chemical Society)

with nanometer detection of proteins, including human serum albumin (HSA), BSA, human IgG, and bovine thrombin [90]. Chang et al. reported a graphene FRET aptasensor for thrombin with a detection limit of 31.3 pM [91]. Wang et al. developed an ultrasensitive (LOD of 0.5 nM) and selective assay for the detection of cyclin A_2, a prognostic indicator in early-stage cancer, using fluorescent-labeled $p^{21(WAF-1)}$ derived from cyclin A_2 binding sequence [92]. Furthermore, similar construction of an aptamer/GO sensor has been demonstrated for in situ adenosine triphosphate (ATP) probing in living cells, with the capability of cellular delivery of DNA (Fig. 8.6) [93].

8.5 Biological Applications of Graphene-based Substrates

8.5.1 Scaffolds for Cell Culture and Differentiation

Graphene-based substrates have been developed for potential applications in tissue engineering. Min's group first utilized GO film as a scaffold for mammalian cell culture [94]. NIH-3T3 mouse fibroblasts seeded on GO film did not display obvious change of cell shape, inhibition of cell adhesion and growth, and abnormal expression of cytoskeletal genes. This work indicated that mammalian cells could attach and proliferate on GO substrate with high gene transfection efficiency, and thereby providing a new insight into development of graphene-based materials for implantable applications.

Based on the above study, graphene-based materials were further explored as promising substrates for multipotent progenitor cells culture and tissue engineering due to the unique physicochemical properties of graphene. Recently, researchers developed graphene-based substrates for mesenchymal stem cells (MSC) [95], neural stem cells (NCS; enhanced differentiation of human neural stem cells into neurons on graphene), and induced pluripotent stem cells (iPSCs) [96] growth and controllable differentiation. By tuning the superficial oxygen content, the mechanics and topography of graphene-based scaffolds and the differentiation of these multipotent progenitor cells could be regulated.

Several groups have explored graphene-based scaffolds for musculoskeletal tissue engineering, as graphene-based substrates could direct MSC differentiation into osteoblast and myoblast. For example, graphene-based materials can pre-concentrate growth agents (serum) and differential inducers (such as β-glycerolphosphate and dexamethasone) through π–π stacking interactions between aromatic rings of these molecules and graphene platform [97]. Graphene and GO substrates could act as pre-concentration platforms for enriching agents in culture medium, and therefore efficiently enhanced MSC attachment, growth, and osteogenic differentiation. MSCs possess the capacity to osteogenic differentiation under favorable mechanical stimuli from the surrounding microenvironments [98, 99]. Nayak et al. [100] also reported promotion of osteogenic differentiation of MSCs induced by graphene substrate. However, they found that this phenomenon was not only because of the collection of another osteogenic inducers (bone morphogenetic protein) but also the stiffness and strain properties of graphene films. They found that differentiation level of MSCs grown on graphene substrates (on Si/SiO_2) were much higher than that of MSCs grown on graphene substrates (on polydimethylsiloxane (PDMS), polyethylene terephthalate (PET), and glass slide). It has been suggested that graphene on softer substrates such as PET and PDMS would impact MSCs differentiation, since the lateral stress of graphene scaffolds could provide appropriate cytoskeletal tension for accelerated osteogenic differentiation. Additionally, GO would induce mouse MSCs myoblast differentiation [101]. A study by Ku et al. indicated that graphene-based platforms could significantly accelerate myogenic differentiation from myogenic protein expression analyses, multinucleate myotube formation, and expression of differentiation-specific genes (MyoD, myogenin, troponin T, and MHC). It has also been found that GO would significantly enhance the myogenic differentiation, which was attributed to the serum protein adsorption and stiffness of graphene.

Graphene substrates can promote NSC adhesion and its differentiation toward neurons, rather than glial cells. Since graphene has a good electrical conductivity, the neural activity of the differentiated cells could be evaluated by electrical stimulation using the graphene electrode [102]. Cheng's group reported that CVD-grown graphene substrate accelerated growth-associated protein-43 (GAP-43) expression, and promoted neurite sprouting and outgrowth of neurons extracted from mouse hippocampal [103]. As the formation of neural network and performance in the assembled neural network is one of the key issues for neural tissue engineering, Cheng et al. further studied its impact on the unique electrical and mechanical properties of graphene. As they demonstrated, the graphene film could support the growth of functional neural circuits and improve the neural performance and electrical signaling in neural network (Fig. 8.7) [104]. Inspired by these investigations, they reported a 3D porous structure based on graphene foam (GF), which could support NSCs growth and keep them at an active proliferation state with an upregulation of Ki67 expression. More importantly, 3D-GFs accelerated NSCs differentiation toward astrocytes and especially neurons [105]. Additionally, they found 3D graphene substrate could remarkably rescue lipopolysaccharide-induced neuro-inflammation, while 2D graphene could not [106].

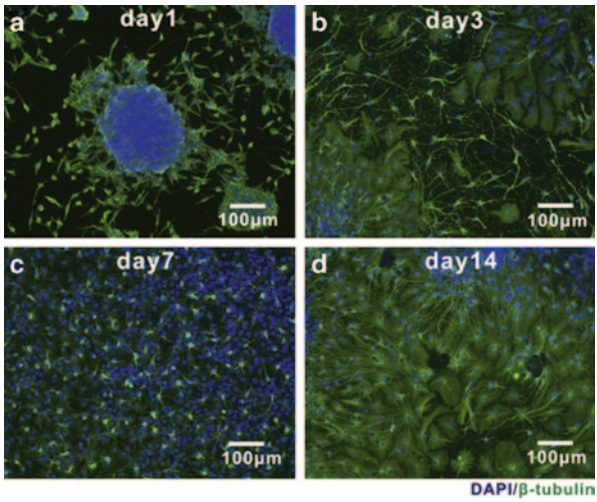

Fig. 8.7 The development of neural networks by NSC differentiation on graphene substrates. (**a–d**) Representative images immunostained by DAPI (nucleus) and antibody against β-tubulin (neurons) at different culturing times (day 1 to day 14). (Adapted with permission from Ref. [104]. Copyright 2013 Elsevier B.V.)

Moreover, graphene (CVD grown) and GO (films made) substrates could support the mouse iPSCs adherence and proliferation [96]. Chen et al. revealed graphene and GO substrates could induce iPSCs spontaneous differentiation into ectodermal and mesodermal lineages; however, they led to distinct differentiation characteristics due to the different surface chemical properties. Graphene suppressed the iPSCs differentiation toward the endodermal lineage, while GO enhanced the endodermal differentiation. All these investigations suggested that graphene-based platforms might find promising applications for stem cell research and tissue engineering with excellent biocompatibility and incredible capability of enhanced differentiation. Although much progress has been made on biomedical applications of graphene-based substrates in tissue regeneration, more efforts should be made on the interactions of biosystems and graphene, such as the long-term in vivo toxicity and immunity after implantation, and efficiency of in vivo tissue repair.

8.5.2 Substrates for Antibacterial Effects

Nowadays, antibacterial nanomaterials, such as silver nanoparticles [107], titanium oxide nanoparticles [108], and carbon nanotubes (CNTs) [109], are widely used in daily life, since they show less drug resistance than the traditional antibiotics. The potential use of graphene-based nanomaterials for antibacterial applications also attracts increasing interests. Fan and Huang's groups explored the antibacterial properties of GO and rGO, which was obtained through modified Hummers' method (Fig. 8.8) [110]. They found that both GO and rGO at low concentration (85 ug/mL) could effectively inhibit the growth of gram-negative bacteria, *Escherichia coli*. The mechanism of antibacterial property is that GO induced cell membrane

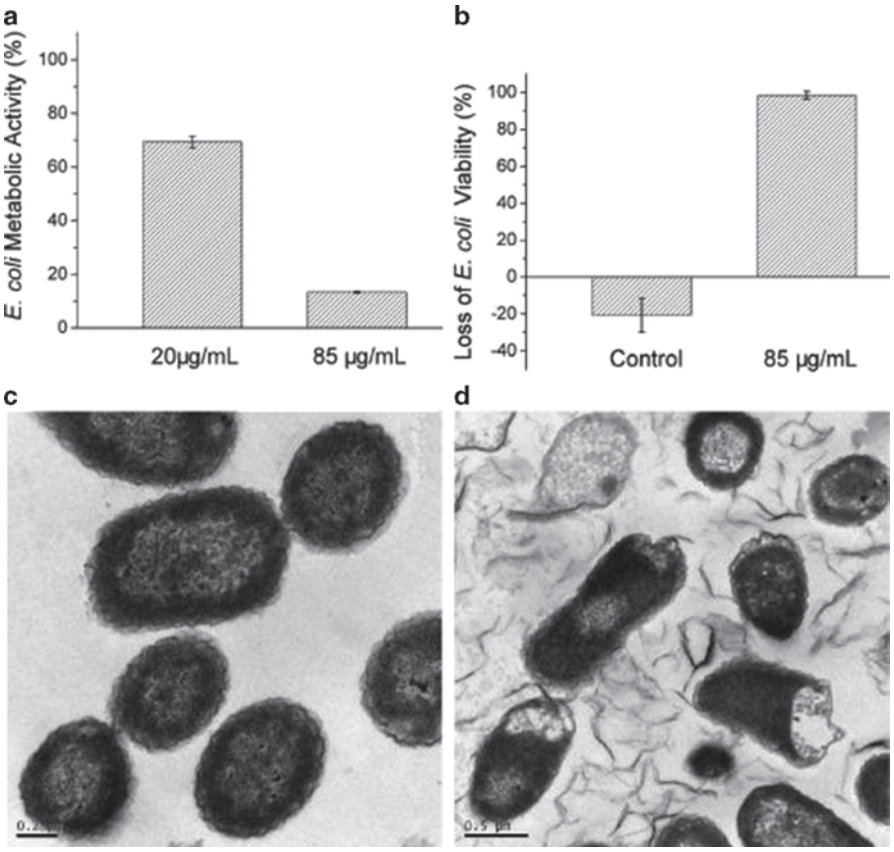

Fig. 8.8 Antibacterial activity of GO nanosheets. Metabolic activity of *E. coli* incubation with GO (**a**), antibacterial activity of GO nanosheets against *E. coli* (**b**), TEM images of *E. coli* (**c**), and *E. coli* exposed to GO nanosheets (**d**). (Adapted with permission from Ref. [110]. Copyright 2010 American Chemical Society)

damage and consequently led to cytoplasm leakage. Moreover, GO and rGO suspensions were conveniently fabricated into macroscopic antibacterial papers via vacuum filtration. Therefore, mass production of antibacterial paper with low cost can be expected with graphene-based materials. Moreover, GO and rGO nanowells showed remarkable destruction of gram-positive bacteria, such as *Staphylococcus aureus*, compared to gram-negative bacteria *E. coli* [111]. Sharp edges of GO or rGO nanowells directly interacted with *S. aureus*, which lacks an outer membrane, and then restrained the activity of microorganism. Besides bacteria, the mycelial growth could be inhibited by rGO nanosheets. Sawangphruk et al. has applied three fungi models, including *Aspergillus niger, Aspergillus oryzae*, and *Fusarium oxysporum* in their study. The IC_{50} values of rGO against three types of fungi were 50, 100, and 100 μg/mL, respectively [112].

The mechanism of antibacterial and antifungal activity of graphene-based materials was suggested mainly in two possible ways [110–113]: (1) GO or rGO damages membrane of microorganisms by theirs sharpened edges, leading to the leakage of cytoplasm. (2) Graphene-based nanomaterials cause the membrane and oxidative stress to induce bacterial toxicity.

On the other hand, there were some controversial reports regarding antimicrobial performance of the graphene-based materials. Das et al. found that GO was not harmful to bacteria, such as *E. coli* and *Pseudomonas aeruginosa* [114]. Similarly, Sun and coworkers demonstrated that GO could enhance the microbial attachment and growth rather than inhibition. However, they did observe that graphene-modified nanoparticles showed an enhanced bacterial toxicity. For instance, *E. coli* adsorbed on the surface of rGO/TiO_2 composite thin film is more sensitive to photoinactivation [115], and GO/Ag complexes showed an enhanced antibacterial activity [116]. Based on the investigation of highly enhanced antibacterial property of GO/Ag complex, Gao et al. have further studied its stability and long-term antibacterial properties. They found that GO/Ag@Fe_2O_3 complexes showed significantly enhanced stability by decreasing the release rate of Ag^+ iron compared to Ag@Fe_2O_3. The presence of GO obviously slowed down the oxidation process of the Ag nanoparticles and enabled Ag^+ ions recrystallization on GO surface, therefore exhibiting long-term antibacterial property against bacteria (both gram negative and gram positive) [117]. This work revealed the origin of enhanced antibacterial effect of nanoparticles combined with GO. Shen's group has coordinated lanthanum (III) on GO sheets (GO–La complexes) for inhibition of *E. coli* growth [118].

8.6 Outlook

Graphene and its derivatives have been extensively studied for their biological applications since 2008. As the encouraging yet preliminary studies show, the large surface area ensures graphene-based nanomaterials as efficient vehicle to transport therapeutics or imaging agents into cells. In addition to active or passive targeting, strong NIR absorbance of graphene facilitates the enhanced cargo accumulation in the tumor sites through light-induced local temperature increase. Graphene's excellent electronic properties make it popular in biological sensing; besides, unique planar structure and physicochemical properties of graphene and GO attract much attention with regard to their use as cell culture scaffolds and anti-bacterial substrates. Clearly, the positive feedbacks of graphene-based biomedical investigations so far will accelerate the research in the related fields, and inspire more explorations of these nanomateirals in biomedical applications. Here, we list several possible directions of biological and medical research on graphene in the future:

1. Development of graphene-based multifunctional delivery systems. There has been a trend of development of nanotheranostic platform based on GO. Future research interests with graphene, especially GO, will be focused on the

applications of GO for co-delivery of multiple therapeutics and/or imaging agents, integration of multiple modalities of clinical purpose, including diagnosis, controlled loading and release of cargoes, targeting, in situ tracking inside cells or tumor sites, and multimodal therapy, for better clinical outcome. In addition, oral transmucosal delivery of non-cancer therapeutics may deserve special attention in the future research.

2. Size-, morphology-, and property-controllable, and scalable production of graphene. Although many synthetic routes of graphene and its derivatives have been developed, a protocol of biocompatible graphene with controlled size, size distribution, and surface nature, as well as scale-up production and fine reproducibility, are urgently demanded. Moreover, inside look into the mechanism of graphene oxidation is currently a priority to rationally optimize the preparation of GO.
3. Biological effects and safety issues of graphene and its derivatives. There are increasing concerns regarding the in vitro and in vivo toxicity of graphene-based nanomaterials, and significant progress has been made to develop biocompatible graphene derivatives through appropriate surface coating and functionalization. However, different and even contrary results reported so far complicate the situation, making it difficult to draw a clear conclusion regarding the toxicity of graphene at in vitro and in vivo levels, because it is defined by purity, size, oxygen content, and surface chemistry of graphene. Therefore, a profound understanding of the interactions between graphene and biosystems, especially the toxicity of graphene nanomaterials, both in vitro and in vivo, is highly desired before their clinical applications.

After all, graphene and its derivatives have shown promising future in the field of biology and medicine, based on numerous efforts and rapidly increasing attention from researcher and the society. Despite facing many problems and challenges at current stage, we have strong faith that the exploration of the biomedical applications of graphene, GO, and its other related derivatives will move forward, and finally reach clinical stages, with strong, continuous, and joint efforts from researchers with backgrounds spanning from materials chemistry, nanotechology, biology, to medicine.

References

1. T. Palacios, Nat. Nanotechnol. **6**, 464 (2011)
2. Y. Liu, X. Dong, P. Chen, Chem. Soc. Rev. **41**, 2283 (2012)
3. D.A. Brownson, D.K. Kampouris, C.E. Banks, J. Power Sources **196**, 4873 (2011)
4. K.S. Novoselov, A.K. Geim, S. Morozov, D. Jiang, Y. Zhang, S. Dubonos, I. Grigorieva, A. Firsov, Science **306**, 666 (2004)
5. D. Cohen-Tanugi, J.C. Grossman, Nano Lett. **12**, 3602 (2012)
6. Z. Liu, J.T. Robinson, S.M. Tabakman, K. Yang, H. Dai, Mater. Today **14**, 316 (2011)
7. H. Shen, L. Zhang, M. Liu, Z. Zhang, Theranostics **2**, 283 (2012)
8. D.R. Dreyer, S. Park, C.W. Bielawski, R.S. Ruoff, Chem. Soc. Rev. **39**, 228 (2010)

9. L. Zhang, J. Xia, Q. Zhao, L. Liu, Z. Zhang, Small **6**, 537 (2010)
10. Y. Chong, Y. Ma, H. Shen, X. Tu, X. Zhou, J. Xu, J. Dai, S. Fan, Z. Zhang, Biomaterials **35**, 5041 (2014)
11. Z. Liu, J.T. Robinson, X. Sun, H. Dai, J. Am. Chem. Soc. **130**, 10876 (2008)
12. J. Huang, C. Zong, H. Shen, Y. Cao, B. Ren, Z. Zhang, Nanoscale **5**, 10591 (2013)
13. Y. Yang, Y.M. Zhang, Y. Chen, D. Zhao, J.T. Chen, Y. Liu, Chem. A. Eur. J. **18**, 4208 (2012)
14. L. Zhang, Z. Lu, Q. Zhao, J. Huang, H. Shen, Z. Zhang, Small **7**, 460 (2011)
15. J. Huang, C. Zong, H. Shen, M. Liu, B. Chen, B. Ren, Z. Zhang, Small **8**, 2577 (2012)
16. C.F. Rochlitz, Swiss Med. Weekly **131**, 4 (2001)
17. L. Naldini, U. Blömer, P. Gallay, D. Ory, R. Mulligan, F.H. Gage, I.M. Verma, D. Trono, Science **272**, 263 (1996)
18 B. Chen, M. Liu, L. Zhang, J. Huang, J. Yao, Z. Zhang, J. Mater. Chem **21**, 7736 (2011)
19. L. Feng, S. Zhang, Z. Liu, Nanoscale **3**, 1252 (2011)
20. H. Kim, R. Namgung, K. Singha, I.-K. Oh, W.J. Kim, Bioconjug. Chem. **22**, 2558 (2011)
21. C.W. Beh, W.Y. Seow, Y. Wang, Y. Zhang, Z.Y. Ong, P.L.R. Ee, Y.-Y. Yang, Biomacromolecules **10**, 41 (2008)
22. H. Bao, Y. Pan, Y. Ping, N.G. Sahoo, T. Wu, L. Li, J. Li, L.H. Gan, Small **7**, 1569 (2011)
23. L. Feng, X. Yang, X. Shi, X. Tan, R. Peng, J. Wang, Z. Liu Small **9**, 1989 (2013)
24. H. Shen, M. Liu, Y. Chong, J. Huang, Z. Zhang, Toxicol. Res. **2**, 379 (2013)
25. K. Yang, S. Zhang, G. Zhang, X. Sun, S.-T. Lee, Z. Liu, Nano Lett. **10**, 3318 (2010)
26. J.T. Robinson, S.M. Tabakman, Y. Liang, H. Wang, H. Sanchez Casalongue, D. Vinh, H. Dai, J. Am. Chem. Soc. **133**, 6825 (2011)
27. K. Yang, J. Wan, S. Zhang, B. Tian, Y. Zhang, Z. Liu, Biomaterials **33**, 2206 (2012)
28. M. Guo, J. Huang, H. Shen, M. zhang, A. Zhu, Y. Li, Y. Deng, H. He, Y. Wang, X. Yang, Z. Zhang, H. Chen, Adv. Func. Mater. **25**, 59 (2015)
29. A.F. Zedan, S. Moussa, J. Terner, G. Atkinson, M.S. El-Shall, ACS nano **7**, 627 (2012)
30. X. Shi, H. Gong, Y. Li, C. Wang, L. Cheng, Z. Liu, Biomaterials **34**, 4786 (2013)
31. Z. Huang, H. Xu, A.D. Meyers, A.I. Musani, L. Wang, R. Tagg, A.B. Barqawi, Y.K. Chen, Technol. Cancer Res. Treat **7**, 309 (2008)
32. C.M. Allen, W.M. Sharman, J.E. Van Lier, J. Porphyrins Phthalocyanines **5**, 161 (2001)
33. P. Huang, C. Xu, J. Lin, C. Wang, X. Wang, C. Zhang, X. Zhou, S. Guo, D. Cui, Theranostics **1**, 240 (2011)
34. P. Rong, K. Yang, A. Srivastan, D.O. Kiesewetter, X. Yue, F. Wang, L. Nie, A. Bhirde, Z. Wang, Z. Liu, Theranostics **4**, 229 (2014)
35. Z.M. Markovic, B.Z. Ristic, K.M. Arsikin, D.G. Klisic, L.M. Harhaji-Trajkovic, B.M. Todorovic-Markovic, D.P. Kepic, T.K. Kravic-Stevovic, S.P. Jovanovic, M.M. Milenkovic, Biomaterials **33**, 7084 (2012)
36. J. Ge, M. Lan, B. Zhou, W. Liu, L. Guo, H. Wang, Q. Jia, G. Niu, X. Huang, H. Zhou, Nat. Commun. **5**, (2014)
37. A. Sahu, W.I. Choi, J.H. Lee, G. Tae, Biomaterials **34**, 6239 (2013)
38. B. Tian, C. Wang, S. Zhang, L. Feng, Z. Liu, ACS Nano **5**, 7000 (2011)
39. C. Xu, D. Yang, L. Mei, Q. Li, H. Zhu, T. Wang, ACS Appl.Mater. Interfaces **5**, 12911 (2013)
40. H. Kim, W.J. Kim, Small **10**, 117 (2014)
41. Y.H. Cao, Y.F. Ma, H.M. Wang, M.X. Zhang, X.L. Tu, H. Shen, J.W. Dai, H.C. Guo, Z.J. Zhang, Adv. Funct. Mater. **24**, 6963 (2014)
42. X. Sun, Z. Liu, K. Welsher, J.T. Robinson, A. Goodwin, S. Zaric, H. Dai, Nano Res. **1**, 203 (2008)
43. P.S. Wate, S.S. Banerjee, A. Jalota-Badhwar, R.R. Mascarenhas, K.R. Zope, J. Khandare, R.D.K. Misra, Nanotechnology **23**, 415101 (2012)
44. Y. Wang, H.-B. Yao, X.-H. Wang, S.-H. Yu, J. Mater. Chem. **21**, 562 (2011)
45. C. Peng, W. Hu, Y. Zhou, C. Fan, Q. Huang, Small **6**, 1686 (2010)
46. M.-L. Chen, J.-W. Liu, B. Hu, M.-L. Chen, J.-H. Wang, Analyst **136**, 4277 (2011)
47. M.-L. Chen, Y.-J. He, X.-W. Chen, J.-H. Wang, Bioconjug. Chem. **24**, 387 (2013)
48. Q. Mei, K. Zhang, G. Guan, B. Liu, S. Wang, Z. Zhang, Chem. Commun. **46**, 7319 (2010)

49. S.H. Hu, Y.W. Chen, W.T. Hung, I.W. Chen, S.Y. Chen Adv. Mater. **24**, 1748 (2012)
50. Y. Wang, H. Wang, D. Liu, S. Song, X. Wang, H. Zhang, Biomaterials **34**, 7715 (2013)
51. L. Zhang, Y. Xing, N. He, Y. Zhang, Z. Lu, J. Zhang, Z. Zhang, J. Nanosci. Nanotechnol. **12**, 2924 (2012)
52. M. Zhang, L. Bai, W. Shang, W. Xie, H. Ma, Y. Fu, D. Fang, H. Sun, L. Fan, M. Han, J. Mater. Chem. **22**, 7461 (2012)
53. M. Nurunnabi, Z. Khatun, G.R. Reeck, D.Y. Lee, Y. Lee, Chem. Commun. (Camb) **49**, 5079 (2013)
54. K. Yang, L. Hu, X. Ma, S. Ye, L. Cheng, X. Shi, C. Li, Y. Li, Z. Liu Adv. Mater. **24**, 1868 (2012)
55. M. Zhang, Y. Cao, Y. Chong, Y. Ma, H. Zhang, Z. Deng, C. Hu, Z. Zhang, ACS Appl. Mater. Interfaces **5**, 13325 (2013)
56. H.-W. Yang, C.-Y. Huang, C.-W. Lin, H.-L. Liu, C.-W. Huang, S.-S. Liao, P.-Y. Chen, Y.-J. Lu, K.-C. Wei, C.-C.M. Ma, Biomaterials **35**, 6534 (2014)
57. Z. Sheng, L. Song, J. Zheng, D. Hu, M. He, M. Zheng, G. Gao, P. Gong, P. Zhang, Y. Ma, Biomaterials **34**, 5236 (2013)
58. Y. Zhang, T.R. Nayak, H. Hong, W. Cai, Nanoscale **4**, 3833 (2012)
59. S. Shi, K. Yang, H. Hong, H.F. Valdovinos, T.R. Nayak, Y. Zhang, C.P. Theuer, T.E. Barnhart, Z. Liu, W. Cai, Biomaterials **34**, 3002 (2013)
60. J. Huang, L. Zhang, B. Chen, N. Ji, F. Chen, Y. Zhang, Z. Zhang, Nanoscale **2**, 2733 (2010)
61. Z. Liu, Z. Guo, H. Zhong, X. Qin, M. Wan, B. Yang, Phys. Chem. Chem. Phys. **15**, 2961 (2013)
62. X. Ma, Q. Qu, Y. Zhao, Z. Luo, Y. Zhao, K.W. Ng, Y. Zhao, J. Mater. Chem. B **1**, 6495 (2013)
63. C. Wang, J. Li, C. Amatore, Y. Chen, H. Jiang, X.M. Wang, Angew. Chem. Int. Ed. **50**, 11644 (2011)
64. H. Xu, H. Dai, G. Chen, Talanta **81**, 334 (2010)
65. Q. Zeng, J. Cheng, L. Tang, X. Liu, Y. Liu, J. Li, J. Jiang, Adv. Funct. Mater. **20**, 3366 (2010)
66. X. Kang, J. Wang, H. Wu, I.A. Aksay, J. Liu, Y. Lin, Biosens. Bioelectron. **25**, 901 (2009)
67. S. Alwarappan, C. Liu, A. Kumar, C.-Z. Li, J. Phys. Chem. C **114**, 12920 (2010)
68. H. Wu, J. Wang, X. Kang, C. Wang, D. Wang, J. Liu, I.A. Aksay, Y. Lin, Talanta **80**, 403 (2009)
69. K.-J. Huang, D.-J. Niu, J.-Y. Sun, C.-H. Han, Z.-W. Wu, Y.-L. Li, X.-Q. Xiong, Colloids Surf. B **82**, 543 (2011)
70. M. Du, T. Yang, K. Jiao, J. Mater. Chem. **20**, 9253 (2010)
71. C.X. Lim, H.Y. Hoh, P.K. Ang, K.P. Loh, Anal. Chem. **82**, 7387 (2010)
72. M. Muti, S. Sharma, A. Erdem, P. Papakonstantinou, Electroanalysis **23**, 272 (2011)
73. B. Su, J. Tang, J. Huang, H. Yang, B. Qiu, G. Chen, D. Tang, Electroanalysis **22**, 2720 (2010)
74. Q. Wei, K. Mao, D. Wu, Y. Dai, J. Yang, B. Du, M. Yang, H. Li, Sens. Actuators B **149**, 314 (2010)
75. S. Hou, M.L. Kasner, S. Su, K. Patel, R. Cuellari, J. Phys. Chem. C **114**, 14915 (2010)
76. L. Tan, K.-G. Zhou, Y.-H. Zhang, H.-X. Wang, X.-D. Wang, Y.-F. Guo, H.-L. Zhang, Electrochem. Commun. **12**, 557 (2010)
77. C. MingáLi, Nanoscale **2**, 1485 (2010)
78. Y. Ohno, K. Maehashi, Y. Yamashiro, K. Matsumoto, Nano Lett. **9**, 3318 (2009)
79. O. Yasuhide, M. Kenzo, I. Koichi, M. Kazuhiko, Japanese J. Appl. Phys **50**, 070120 (2011)
80. M. Yang, S. Gong, Chem. Commun **46**, 5796 (2010)
81. G.-B.S.-B.R. Biodevice, D. Transistor, Nano Lett. **8**, 4469 (2008)
82. X. Dong, Y. Shi, W. Huang, P. Chen, L.J. Li, Adv. Mater. **22**, 1649 (2010)
83. T. Cohen-Karni, Q. Qing, Q. Li, Y. Fang, C.M. Lieber, Nano Lett. **10**, 1098 (2010)
84. Q. He, H.G. Sudibya, Z. Yin, S. Wu, H. Li, F. Boey, W. Huang, P. Chen, H. Zhang, ACS Nano **4**, 3201 (2010)
85. R. Kempaiah, A. Chung, V. Maheshwari, ACS Nano **5**, 6025 (2011)
86. Z. Tang, H. Wu, J.R. Cort, G.W. Buchko, Y. Zhang, Y. Shao, I.A. Aksay, J. Liu, Y. Lin, Small **6**, 1205 (2010)

87. C.H. Lu, J. Li, J.J. Liu, H.H. Yang, X. Chen, G.N. Chen, Chem. A. Eur. J. **16**, 4889 (2010)
88. J.W. Yi, J. Park, N.J. Singh, I.J. Lee, K.S. Kim, B.H. Kim, Bioorg. Med. Chem. Lett. **21**, 704 (2011)
89. S. He, B. Song, D. Li, C. Zhu, W. Qi, Y. Wen, L. Wang, S. Song, H. Fang, C. Fan, Adv. Funct. Mater. **20**, 453 (2010)
90. M.J. Aldegunde, L. Castedo, J.R. Granja, Chem. A. Eur. J. **15**, 4785 (2009)
91. H. Chang, L. Tang, Y. Wang, J. Jiang, J. Li, Anal. Chem. **82**, 2341 (2010)
92. X. Wang, C. Wang, K. Qu, Y. Song, J. Ren, D. Miyoshi, N. Sugimoto, X. Qu, Adv. Funct. Mater. **20**, 3967 (2010)
93. Y. Wang, Z. Li, D. Hu, C.-T. Lin, J. Li, Y. Lin, J. Am. Chem. Soc. **132**, 9274 (2010)
94. S.-R. Ryoo, Y.-K. Kim, M.-H. Kim, D.-H. Min, ACS Nano **4**, 6587 (2010)
95. H. Fan, L. Wang, K. Zhao, N. Li, Z. Shi, Z. Ge, Z. Jin, Biomacromolecules **11**, 2345 (2010)
96. G.-Y. Chen, D.-P. Pang, S.-M. Hwang, H.-Y. Tuan, Y.-C. Hu, Biomaterials **33**, 418 (2012)
97. W.C. Lee, C.H.Y. Lim, H. Shi, L.A. Tang, Y. Wang, C.T. Lim, K.P. Loh, ACS Nano **5**, 7334 (2011)
98. A.J. Engler, S. Sen, H.L. Sweeney, D.E. Discher, Cell **126**, 677 (2006)
99. M.F. Pittenger, A.M. Mackay, S.C. Beck, R.K. Jaiswal, R. Douglas, J.D. Mosca, M.A. Moorman, D.W. Simonetti, S. Craig, D.R. Marshak, Science **284**, 143 (1999)
100. T.R. Nayak, H. Andersen, V.S. Makam, C. Khaw, S. Bae, X. Xu, P.-L.R. Ee, J.-H. Ahn, B.H. Hong, G. Pastorin, ACS Nano **5**, 4670 (2011)
101. S.H. Ku, C.B. Park Biomaterials **34**, 2017 (2013)
102. S.Y. Park, J. Park, S.H. Sim, M.G. Sung, K.S. Kim, B.H. Hong, S. Hong, Adv. Mater. **23**, H263 (2011)
103. N. Li, X. Zhang, Q. Song, R. Su, Q. Zhang, T. Kong, L. Liu, G. Jin, M. Tang, G. Cheng, Biomaterials **32**, 9374 (2011)
104. M. Tang, Q. Song, N. Li, Z. Jiang, R. Huang, G. Cheng, Biomaterials **34**, 6402 (2013)
105. N. Li, Q. Zhang, S. Gao, Q. Song, R. Huang, L. Wang, L. Liu, J. Dai, M. Tang, G. Cheng Sci. Rep. **3**, 1604 (2013)
106. Q. Song, Z. Jiang, N. Li, P. Liu, L. Liu, M. Tang, G. Cheng Biomaterials 2014
107. J.S. Kim, E. Kuk, K.N. Yu, J.-H. Kim, S.J. Park, H.J. Lee, S.H. Kim, Y.K. Park, Y.H. Park, C.-Y. Hwang, Nanomed. Nanotechnol. Biol. Med. **3**, 95 (2007)
108. C. Wei, W.Y. Lin, Z. Zainal, N.E. Williams, K. Zhu, A.P. Kruzic, R.L. Smith, K. Rajeshwar, Environ. Sci. Technol. **28**, 934 (1994)
109. S. Kang, M. Herzberg, D.F. Rodrigues, M. Elimelech, Langmuir **24**, 6409 (2008)
110. W. Hu, C. Peng, W. Luo, M. Lv, X. Li, D. Li, Q. Huang, C. Fan, ACS Nano **4**, 4317 (2010)
111. O. Akhavan, E. Ghaderi, ACS Nano **4**, 5731 (2010)
112. M. Sawangphruk, P. Srimuk, P. Chiochan, T. Sangsri, P. Siwayaprahm, Carbon **50**, 5156 (2012)
113. S. Liu, T.H. Zeng, M. Hofmann, E. Burcombe, J. Wei, R. Jiang, J. Kong, Y. Chen, ACS Nano **5**, 6971 (2011)
114. M.R. Das, R.K. Sarma, R. Saikia, V.S. Kale, M.V. Shelke, P. Sengupta, Colloids Surf., B **83**, 16 (2011)
115. O. Akhavan, E. Ghaderi J. Phys. Chem. C, **113**, 20214 (2009)
116. W.-P. Xu, L.-C. Zhang, J.-P. Li, Y. Lu, H.-H. Li, Y.-N. Ma, W.-D. Wang, S.-H. Yu, J. Mater. Chem. **21**, 4593 (2011)
117. N. Gao, Y. Chen, J. Jiang, ACS Appl. Mater Interfaces **5**, 11307 (2013)
118. X. Wang, N. Zhou, J. Yuan, W. Wang, Y. Tang, C. Lu, J. Zhang, J. Shen, J. Mater. Chem. **22**, 1673 (2012)